Journal of the Brazilian Society of Mechanical Sciences and Engineering (2022) 44:335
https://doi.org/10.1007/s40430-022-03634-4

TECHNICAL PAPER

Dynamic modeling and control of a spherical pendulum with a VSCMG

João Francisco Silva Trentin[1] · Davi A. Santos[1] · Samuel da Silva[2] · Hanspeter Schaub[3]

Received: 31 January 2022 / Accepted: 17 June 2022

Abstract
The study of inverted pendulum configurations has attracted the attention of researchers during many decades. One of the main reasons is that inverted-pendulum models have the feature of approximating the dynamics of many real-world mechanisms. Therefore, this paper presents the detailed dynamic modeling and control of a novel spherical pendulum with a variable speed control moment gyroscope. The dynamic model is obtained from the generic 3D pendulum, and the necessary assumptions to model the spherical pendulum are conducted in order to avoid singularities. Furthermore, a proportional-derivative nonlinear controller based on Lyapunov theory is designed to use favorably the features of the variable speed control moment gyroscope to control the spherical pendulum combining the gyroscopic torque and the torque provided by the reaction wheel. The proposed dynamic model and nonlinear controller are evaluated through numerical simulations for two different scenarios, driving the pendulum to a sequence of attitude commands including the upright position and tracking a desired trajectory. The results have shown that the proposed model is nonsingular and that the control law has provided adequate rates controlling the pendulum in both scenarios.

Keywords Spherical pendulum · Nonlinear dynamics · Variable speed control moment gyroscope (VSCMG) · Control

1 Introduction

Inverted pendulum-like systems have many interesting characteristics that drive the research development in dynamics and control throughout the last decades. Many of the features investigated on these systems rely on different real-world applications. Different benchmarks are considered in order to explore and understand different characteristics leading to the proposition of novel pendulum configurations which, in turn, represent various applications, for some examples, see [1–12]

Among the inverted pendulum-like configurations, we highlight the 3D pendulum discussed in [2]. Shen et al. [2] have analyzed the 3D pendulum configuration that consists of a rigid body fixed to a pivot and allows three rotational degrees of freedom. The gravity acts on this rigid body, and three control torques are considered, one for each direction. Moreover, they demonstrate that symmetry assumptions can lead this 3D pendulum configuration to the planar 1D pendulum and to the 2D spherical pendulum.

Based on the control problems proposed in [2], Chaturvedi et al. [13] investigate stabilization problems for the 3D pendulum using a reduced model, proposing two different strategies, one based only on angular velocity feedback and

Technical editor: Wallace Moreira Bessa.

✉ João Francisco Silva Trentin
joaotrentin@ita.br

Davi A. Santos
davists@ita.br

Samuel da Silva
samuel.silva13@unesp.br

Hanspeter Schaub
hanspeter.schaub@colorado.edu

[1] Division of Mechanical Engineering, Department of Mechatronics, Aeronautics Institute of Technology (ITA), P. Mal. Eduardo Gomes, 50, São José dos Campos, SP, Brazil

[2] Department of Mechanical Engineering, School of Engineering of Ilha Solteira, São Paulo State University (UNESP), Av. Brasil, 56, Ilha Solteira, SP, Brazil

[3] Department of Aerospace Engineering Sciences, Colorado Center for Astrodynamics Research, University of Colorado at Boulder, 3775 Discover Drive, 429, Boulder, CO, USA

Published online: 13 July 2022

the other based on angular velocity and reduced attitude. Chaturvedi and McClamroch [14] formalize the asymptotic stabilization of the hanging equilibrium manifold and discuss the closed-loop dynamics of the 3D pendulum controlled by angular velocity feedback. Chaturvedi and McClamroch [15] derive a continuous controller based on novel Lyapunov functions suited for attitude stabilization problems in the special orthogonal group that takes into account saturation in the control torque. Chaturvedi et al. [16] have shown the stabilization in the case where the 3D pendulum is axially symmetric, and the center of mass lies on the axis of symmetry. The problems studied in [16] can be viewed as the stabilization of a Lagrange top or as the stabilization of a spherical pendulum, depending on some considerations. The results show that the stabilization in the hanging and inverted position is effective, although with very large control torques. More recently, a neural-network-based fuzzy logic control of a 3D pendulum is considered in [17] and Yao [18] presents a robust adaptive finite-time attitude tracking control of the 3D pendulum. Real-time experiments are conducted, and external disturbances are applied to the system to verify its robust performance. There are some gaps in these works that must be bridged, such as different ways of actuating the 3D pendulum once the majority of them assume three control torques directly applied to each of the rotational degrees of freedom.

Considering the concepts of the 3D pendulum, Gajamohan et al. [19] have introduced the Cubli, which is a mechatronic cube that can jump up and balance using three orthogonal body-fixed reaction wheels. Muehlebach and D'Andrea [5] carry out the nonlinear analysis and control of the Cubli detailing this system's main features. The authors have found a reduced description of the dynamics that is used for control design. The design of two nonlinear control strategies is presented, and the results have been verified experimentally.

Moreover, the use of the gyroscopic effect to aid in the control of inverted pendulum-like systems has also been deeply investigated. It is well known that control moment gyroscopes (CMGs) can produce high magnitude torque with a small variation in the gimbal angle, and this feature can be very useful for the control of many dynamical systems. Recently, single-wheel robot [20], bicycle [21, 22], wheeled inverted pendulum [23], sphere robots [24], balance assistance systems [25, 26], among others [27–30] have been studied in situations where the gyroscopic effect generated using CMGs is used to stabilize these systems aiding in their balancing so they can follow a desired trajectory or resist to external disturbances.

Therefore, many different applications of the gyroscopic effect taking advantage of the torque amplification capacity can be found in the literature as mentioned above. Although CMGs have many interesting characteristics that aid in the control of dynamic systems, it is known that they can reach singularities that can result on gimbal locks. An interesting alternative is to use variable speed control moment gyroscopes (VSCMGs). The use of VSCMG is a well-established way to stabilize spacecrafts [31]. In this case, it is allowed to control the spin rate of the wheel, not only the gimbal rate. Thus, the VSCMG provides two different control torques in a single actuator.

Trentin et al. [7] have discussed the use of a VSCMG to control an inverted pendulum comparing the results to the classical reaction wheel pendulum; however, the motion was restricted to the plane. Thus, the primary contribution of this paper is to extend the previous results and to propose a novel pendulum configuration controlled by a VSCMG actuator. This work couples the dynamic model provided by the 3D pendulum used to yield a spherical pendulum to the interesting features of a VSCMG actuator. The focus of this paper is to obtain a nonsingular model of a spherical pendulum that can be stabilized in the upright position and track a desired reference. Some assumptions and remarks are made to properly obtain the model of an spherical pendulum from the 3D pendulum. To the best of the authors' knowledge, this is the first investigation of the control of a VSCMG-actuated spherical pendulum. The dynamic model is derived using the modified Rodrigues parameters to describe the attitude and is based on the Newton–Euler method to obtain the equation of motion. Moreover, the control law is derived based on Lyapunov theory providing an adequate motion for the VSCMG. It is important to state that in the case presented in this study, the pendulum is allowed to rotate in two degrees of freedom. Many of the studies regarding gyroscopically controlled inverted pendulum restrict the motion to only one degree of freedom. Additionally, we explicitly show the control effort needed for controlling the pendulum in the inverted position. Some of the works do not present these values, which makes it very difficult to verify if the approach presented by them is possible to be tested in a practical experiment. In summary, the contributions of this work are: (1) the dynamic modeling of a novel VSCMG-actuated spherical pendulum, (2) the design of a control law suitable for such system, and (3) the evaluation through numerical simulation of the proposed model and controller.

The paper is organized as follows: Section 2 presents the complete derivation of a dynamic model of the proposed VSCMG-actuated pendulum using modified Rodrigues parameters (MRPs), shows the assumptions to yield the spherical pendulum, and provides the error dynamics. Section 3 comprises the design of the control strategy that assures global asymptotic stabilization of the system. Section 4 shows the numerical results obtained for two scenarios, controlling the spherical pendulum in a sequence of attitude commands and tracking a desired command. Finally, Sect. 5 draws the conclusions.

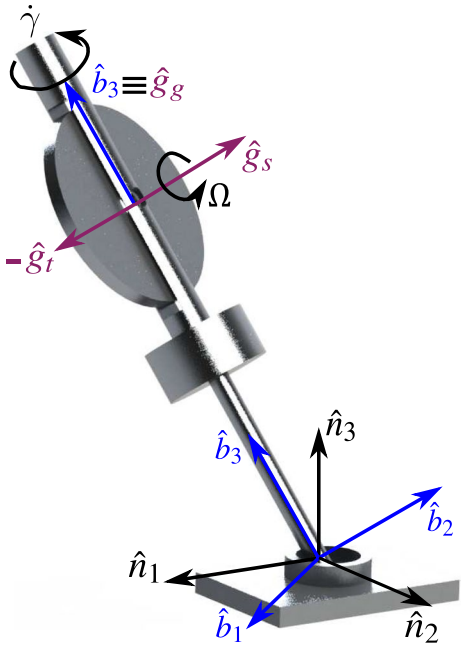

Fig. 1 Spherical pendulum actuated by a VSCMG

2 Dynamic modeling

This section presents the notation used in the paper, the complete derivation of the model of a 3D pendulum with a VSCMG, shown in Fig. 1, and how this model can lead to a spherical pendulum. The modified Rodrigues parameters are used to describe the attitude of this new pendulum configuration in a way to avoid singularities, once the shadow set property of the MRPs allows a complete three-dimensional nonsingular attitude description [31, 32].

2.1 Notation

Denote the set of real numbers by $\mathbb{R}$, the special orthogonal group by SO(3), and the 2-sphere by $\mathbb{S}^2$. Denote the unit vectors as $\hat{\mathbf{a}}$, and the algebraic vectors are denoted in bold format, e.g, $\mathbf{a} \in \mathbb{R}^3$. Matrices are denoted by $[A]$. The relation between representations can be written as ${}^{B}\mathbf{b} = [BN]^{N}\mathbf{n}$, where $[BN] \in \text{SO}(3)$ is the attitude matrix of B with respect to (w.r.t.) N and the superscript indicates the frame in which the vector is taken. Sometimes it is necessary to define a physical quantity in one frame w.r.t. another one. In this case, a subscript is added to the vector quantity, e.g., $\mathbf{a}_{b/n}$. The ith component of $\mathbf{a}$ is denoted by a_i. Now, consider two vectors $\mathbf{a} = \{a_1\ a_2\ a_3\}^T$ and $\mathbf{b}$ taken in the same representation and denote the vector product by the matrix multiplication $[\mathbf{a}\times]\mathbf{b}$, where the skew-symmetric matrix $[\mathbf{a}\times]$ is defined as

$$[\mathbf{a}\times] = \begin{bmatrix} 0 & -a_3 & a_2 \\ a_3 & 0 & -a_1 \\ -a_2 & a_1 & 0 \end{bmatrix}. \tag{1}$$

2.2 Reference frames definitions and kinematics

Firstly, consider the following coordinate frames: the inertial one defined as $N \triangleq \{\hat{\mathbf{n}}_1, \hat{\mathbf{n}}_2, \hat{\mathbf{n}}_3\}$, the body-fixed frame given by $B \triangleq \{\hat{\mathbf{b}}_1, \hat{\mathbf{b}}_2, \hat{\mathbf{b}}_3\}$, the gimbal-fixed frame denoted by $G \triangleq \{\hat{\mathbf{g}}_s, \hat{\mathbf{g}}_t, \hat{\mathbf{g}}_g\}$, and consider the reference one $R \triangleq \{\hat{\mathbf{r}}_1, \hat{\mathbf{r}}_2, \hat{\mathbf{r}}_3\}$. Note that $\hat{\mathbf{g}}_g$ is aligned with $\hat{\mathbf{b}}_3$, as shown in Fig. 1. As seen from B, $\hat{\mathbf{g}}_s$ and $\hat{\mathbf{g}}_t$ are time varying; they are

$$\hat{\mathbf{g}}_s(t) = \cos(\gamma(t) - \gamma_0)\hat{\mathbf{g}}_s(t_0) + \sin(\gamma(t) - \gamma_0)\hat{\mathbf{g}}_t(t_0), \tag{2}$$

$$\begin{aligned} \hat{\mathbf{g}}_t(t) = &- \sin(\gamma(t) - \gamma_0)\hat{\mathbf{g}}_s(t_0) \\ &+ \cos(\gamma(t) - \gamma_0)\hat{\mathbf{g}}_t(t_0), \end{aligned} \tag{3}$$

where $\gamma(t)$ denotes the gimbal angle varying with time and γ_0 is an initial gimbal angle. $[BG]$ is defined as $[BG] = [\hat{\mathbf{g}}_s\ \hat{\mathbf{g}}_t\ \hat{\mathbf{g}}_g]$.

The 3D pendulum is a rigid body with three rotational degrees of freedom, fixed at a pivot point and subject to gravity [2, 16, 18]. The angular velocity of the 3D pendulum in the body-frame w.r.t. inertial frame is $\boldsymbol{\omega}_{b/n} = \{\omega_1, \omega_2, \omega_3\}$. The angular velocity of the gimbal in the G frame relative to B is given by ${}^{G}\boldsymbol{\omega}_{g/b} = \dot{\gamma}\hat{\mathbf{g}}_g$, and the reaction wheel angular velocity is ${}^{G}\boldsymbol{\omega}_{w/g} = \Omega\hat{\mathbf{g}}_s$. For simplicity, all quantities that do not present superscript are taken in the body frame B.

The MRP $\boldsymbol{\sigma} \in \mathbb{R}^3$ is defined as

$$\boldsymbol{\sigma} \triangleq \tan\frac{\Phi}{4}\hat{\mathbf{e}}, \tag{4}$$

where $\Phi \in (-2\pi, 2\pi)$ is the principal rotation angle, $\hat{\mathbf{e}}$ is the principal axis referring to the Euler's principal rotation theorem [31, 32]. The MRPs are singular at $\Phi = \pm 2\pi$. However, this singularity can be avoided if the MRP set is switched to its shadow set, thus leading to a complete nonsingular three-dimensional attitude description [31]. Mathematically, when $\boldsymbol{\sigma}^T\boldsymbol{\sigma} > 1$, the MRP set is mapped to the shadow set given by

$$\boldsymbol{\sigma}^S \triangleq -\frac{\boldsymbol{\sigma}}{\boldsymbol{\sigma}^T\boldsymbol{\sigma}}. \tag{5}$$

The kinematic differential equation of MRPs is [31]:

$$\dot{\boldsymbol{\sigma}}_{b/n} = \frac{1}{4}[B(\boldsymbol{\sigma}_{b/n})]\boldsymbol{\omega}_{b/n}, \tag{6}$$

where $\dot{\boldsymbol{\sigma}}_{b/n} \in \mathbb{R}^3$ denotes the rate of the MRP in the body frame taken w.r.t. inertial frame, and the matrix $[B(\boldsymbol{\sigma}_{b/n})] \in \mathbb{R}^{3\times3}$ is given by

$$[B(\boldsymbol{\sigma}_{b/n})] = [(1 - \boldsymbol{\sigma}_{b/n}^T \boldsymbol{\sigma}_{b/n})[I_{3\times3}] + 2[\boldsymbol{\sigma}_{b/n}\times] + 2\boldsymbol{\sigma}_{b/n}\boldsymbol{\sigma}_{b/n}^T]. \tag{7}$$

Furthermore, it is necessary to define three inertia matrices to model the 3D pendulum equipped with a VSCMG. The inertia matrix of the 3D pendulum $[I_s]$ contains the inertias of the body and of the VSCMG calculated relative to the overall center of mass. It is given in the B frame, and it is constant as seen from the B frame. The inertia matrix of the gimbal ${}^G[I_G]$ is defined in the gimbal frame as ${}^G[I_G] = \text{ diag } (I_{Gs}, I_{Gt}, I_{Gg})$. The inertia matrix of the reaction wheel is already presented in the gimbal frame due to the disk symmetry denoted by ${}^G[I_W] = \text{ diag } (I_{ws}, I_{wt}, I_{wt})$. These two matrices need to be rotated to the body frame, where they are time-varying, yielding

$$\begin{aligned} {}^B[I_G] &= [BG]^G[I_G][BG]^T, \\ {}^B[I_G] &= I_{Gs}\hat{\mathbf{g}}_s\hat{\mathbf{g}}_s^T + I_{Gt}\hat{\mathbf{g}}_t\hat{\mathbf{g}}_t^T + I_{Gg}\hat{\mathbf{g}}_g\hat{\mathbf{g}}_g^T, \\ {}^B[I_W] &= [BG]^G[I_W][BG]^T, \end{aligned} \tag{8}$$

$${}^B[I_W] = I_{ws}\hat{\mathbf{g}}_s\hat{\mathbf{g}}_s^T + I_{wt}\hat{\mathbf{g}}_t\hat{\mathbf{g}}_t^T + I_{wt}\hat{\mathbf{g}}_g\hat{\mathbf{g}}_g^T. \tag{9}$$

Later on, it might be convenient sometimes to express the inertia matrices of the gimbal and of the reaction wheel as a single inertia matrix of the VSCMG denoted by ${}^G[J] = {}^G[I_G] + {}^G[I_W]$. Moreover, the total inertia matrix $[I]$ in the body frame can be expressed as

$$[I] = [I_s] + J_s\hat{\mathbf{g}}_s\hat{\mathbf{g}}_s^T + J_t\hat{\mathbf{g}}_t\hat{\mathbf{g}}_t^T + J_g\hat{\mathbf{g}}_g\hat{\mathbf{g}}_g^T. \tag{10}$$

2.3 Equation of motion

To obtain the equation of motion of the 3D pendulum with a VSCMG, the angular momentum of the 3D pendulum $\mathbf{h}_B$, of the gimbal $\mathbf{h}_G$, and of the reaction wheel $\mathbf{h}_W$ must be evaluated to yield the total angular momentum of the complete system around the center of mass

$$\mathbf{h} = \mathbf{h}_B + \mathbf{h}_G + \mathbf{h}_W. \tag{11}$$

The angular momentum of the body is given by

$$\mathbf{h}_B = [I_s]\boldsymbol{\omega}_{b/n}. \tag{12}$$

The gimbal frame angular momentum is

$$\mathbf{h}_G = [I_G]\boldsymbol{\omega}_{g/n}, \tag{13}$$

where $\boldsymbol{\omega}_{g/n} = \boldsymbol{\omega}_{g/b} + \boldsymbol{\omega}_{b/n}$. Using the definitions for the inertia matrix and for the angular velocities, the angular momentum of the gimbal frame can be written as

$$\mathbf{h}_G = \left(I_{Gs}\hat{\mathbf{g}}_s\hat{\mathbf{g}}_s^T + I_{Gt}\hat{\mathbf{g}}_t\hat{\mathbf{g}}_t^T + I_{Gg}\hat{\mathbf{g}}_g\hat{\mathbf{g}}_g^T\right)\boldsymbol{\omega}_{b/n} + I_{Gg}\dot{\gamma}\hat{\mathbf{g}}_g. \tag{14}$$

Here, we introduce the projection of $\boldsymbol{\omega}_{b/n}$ onto the G frame unit axes, where $\omega_s = \hat{\mathbf{g}}_s^T\boldsymbol{\omega}_{b/n}$, $\omega_t = \hat{\mathbf{g}}_t^T\boldsymbol{\omega}_{b/n}$, and $\omega_g = \hat{\mathbf{g}}_g^T\boldsymbol{\omega}_{b/n}$. These relations help to simplify many steps of the derivation of this model, and they are also used in the design of the controller. They allow the angular momentum of the gimbal to be written as

$$\mathbf{h}_G = I_{Gs}\omega_s\hat{\mathbf{g}}_s + I_{Gt}\omega_t\hat{\mathbf{g}}_t + I_{Gg}(\omega_g + \dot{\gamma})\hat{\mathbf{g}}_g. \tag{15}$$

The angular momentum of the reaction wheel is given by

$$\mathbf{h}_W = [I_W]\boldsymbol{\omega}_{w/n}, \tag{16}$$

where $\boldsymbol{\omega}_{w/n} = \boldsymbol{\omega}_{w/g} + \boldsymbol{\omega}_{g/b} + \boldsymbol{\omega}_{b/n}$. Analogously to what was done for the gimbal angular momentum, the reaction wheel angular momentum can be written as

$$\mathbf{h}_W = I_{ws}(\omega_s + \Omega)\hat{\mathbf{g}}_s + I_{wt}\omega_t\hat{\mathbf{g}}_t + I_{wt}(\omega_g + \dot{\gamma})\hat{\mathbf{g}}_g. \tag{17}$$

The Euler's equation is used to derive the equation of motion of the 3D pendulum with a VSCMG. The inertial derivative of the total angular momentum is calculated and equaled to the external torques acting on the system

$$\dot{\mathbf{h}} = \boldsymbol{\ell}, \tag{18}$$

where $\boldsymbol{\ell} = -mg\mathbf{r}_{cm} \times [BN]\hat{n}_3$ denotes the external torque that gravity exerts onto the system, where m is the mass of the system, g the acceleration of gravity, $\mathbf{r}_{cm} \in \mathbb{R}^3$ the center of mass vector, $[BN]$ is the attitude matrix of the body frame w.r.t. inertial one, and $\hat{n}_3$ the inertial direction in which gravity acts.

We recommend to evaluate the inertial derivatives of the gimbal frame's angular momentum and the reaction wheel first. With these results, they are combined with the inertial derivative of the body angular momentum to yield the total inertial derivative of $\mathbf{h}$. Thus, they are added together and equaled to the external torques acting onto the system to yield the equation of motion. To simplify the notation, from this point onwards $\boldsymbol{\omega} = \boldsymbol{\omega}_{b/n}$.

Note that the vectors $\hat{\mathbf{g}}_s$, $\hat{\mathbf{g}}_t$, and $\hat{\mathbf{g}}_g$ appear in the angular momentum of the gimbal and of the reaction wheel. Therefore, the inertial derivatives of these vectors must be evaluated

$$\dot{\hat{\mathbf{g}}}_s = {}^B\frac{\mathrm{d}}{\mathrm{d}t}(\hat{\mathbf{g}}_s) + \boldsymbol{\omega} \times \hat{\mathbf{g}}_s = (\dot{\gamma} + \omega_g)\hat{\mathbf{g}}_t - \omega_t\hat{\mathbf{g}}_g, \tag{19}$$

$$\dot{\hat{\mathbf{g}}}_t = {}^B\frac{\mathrm{d}}{\mathrm{d}t}(\hat{\mathbf{g}}_t) + \boldsymbol{\omega} \times \hat{\mathbf{g}}_t = -(\dot{\gamma} + \omega_g)\hat{\mathbf{g}}_s - \omega_s\hat{\mathbf{g}}_g, \tag{20}$$

$$\dot{\hat{\mathbf{g}}}_g = \frac{^B \mathrm{d}}{\mathrm{dt}}(\hat{\mathbf{g}}_g) + \boldsymbol{\omega} \times \hat{\mathbf{g}}_g = \omega_t \hat{\mathbf{g}}_s - \omega_s \hat{\mathbf{g}}_t. \tag{21}$$

Additionally, it is important to evaluate the inertial derivatives of the G frame body angular velocities

$$\dot{\omega}_s = \dot{\hat{\mathbf{g}}}_s^T \boldsymbol{\omega} + \hat{\mathbf{g}}_s^T \dot{\boldsymbol{\omega}} = \dot{\gamma}\omega_t + \hat{\mathbf{g}}_s^T \dot{\boldsymbol{\omega}}, \tag{22}$$

$$\dot{\omega}_t = \dot{\hat{\mathbf{g}}}_t^T \boldsymbol{\omega} + \hat{\mathbf{g}}_t^T \dot{\boldsymbol{\omega}} = -\dot{\gamma}\omega_s + \hat{\mathbf{g}}_t^T \dot{\boldsymbol{\omega}}, \tag{23}$$

$$\dot{\omega}_g = \dot{\hat{\mathbf{g}}}_g^T \boldsymbol{\omega} + \hat{\mathbf{g}}_g^T \dot{\boldsymbol{\omega}} = \hat{\mathbf{g}}_g^T \dot{\boldsymbol{\omega}}. \tag{24}$$

All the expressions developed here are used to derive the inertial derivatives of $\mathbf{h}_W$ and $\mathbf{h}_G$. Thus, the inertial derivative of the $\mathbf{h}_W$ is given by

$$\begin{aligned}\dot{\mathbf{h}}_W =& \hat{\mathbf{g}}_s(I_{ws}(\dot{\Omega} + \dot{\gamma}\omega_t + \hat{\mathbf{g}}_s^T \dot{\omega})) \\ &+ \hat{\mathbf{g}}_t([I_{ws}(\dot{\gamma}(\omega_s + \Omega) + \Omega\omega_g) + I_{wt}\hat{\mathbf{g}}_t^T \dot{\omega} \\ &+ (I_{ws} - I_{wt})\omega_s\omega_g - 2I_{wt}\omega_s\dot{\gamma}) + \hat{\mathbf{g}}_g(I_{wt}(\hat{\mathbf{g}}_g^T \dot{\omega} + \ddot{\gamma}) \\ &+ (I_{wt} - I_{ws})\omega_s\omega_t - I_{ws}\Omega\omega_t).\end{aligned} \tag{25}$$

Analyzing this result in the format of Euler's equation $\dot{\mathbf{h}}_W = \boldsymbol{\ell}_W$, where $\boldsymbol{\ell}_W$ is the torque that the gimbal frame exerts on the reaction wheel, note that the torque component around $\hat{\mathbf{g}}_s$ has to be produced by the motor that spins the reaction wheel. Thus, the reaction wheel motor torque is expressed as

$$u_s = I_{ws}(\dot{\Omega} + \hat{\mathbf{g}}_s^T \dot{\boldsymbol{\omega}} + \dot{\gamma}\omega_t). \tag{26}$$

Using the expressions defined from Eqs. (19)–(24), the inertial derivative of the gimbal frame angular momentum is obtained as

$$\begin{aligned}\dot{\mathbf{h}}_G =& \hat{\mathbf{g}}_s((I_{Gs} - I_{Gt} + I_{Gg})\dot{\gamma}\omega_t + I_{Gs}\hat{\mathbf{g}}_s^T \dot{\boldsymbol{\omega}} \\ &+ (I_{Gg} - I_{Gt})\omega_t\omega_g) + \hat{\mathbf{g}}_t((I_{Gs} - I_{Gt} - I_{Gg})\dot{\gamma}\omega_s \\ &+ I_{Gt}\hat{\mathbf{g}}_t^T \dot{\boldsymbol{\omega}} + (I_{Gs} - I_{Gg})\omega_s\omega_g) + \hat{\mathbf{g}}_g(I_{Gg}(\hat{\mathbf{g}}_g^T \dot{\boldsymbol{\omega}} + \ddot{\gamma}) \\ &+ (I_{Gt} - I_{Gs})\omega_s\omega_t).\end{aligned} \tag{27}$$

Now, we need to analyze the gimbal and the reaction wheel together. For this end, let us write Euler's equation as

$$\dot{\mathbf{h}}_G + \dot{\mathbf{h}}_W = \boldsymbol{\ell}_G. \tag{28}$$

Considering that $\boldsymbol{\ell}_G$ is the torque vector exerted by the 3D pendulum onto the VSCMG and noting that the component around $\hat{\mathbf{g}}_g$ has to be provided by the motor responsible for gimbaling the CMG. The motor torque u_g of the gimbal is given by

$$u_g = J_g(\hat{\mathbf{g}}_g^T \dot{\boldsymbol{\omega}} + \ddot{\gamma}) - (J_s - J_t)\omega_s\omega_t - I_{ws}\Omega\omega_t. \tag{29}$$

Finally, the inertial derivative of the body angular momentum is given by

$$\dot{\mathbf{h}}_B = [I_s]\dot{\boldsymbol{\omega}} + \boldsymbol{\omega} \times [I_s]\boldsymbol{\omega}. \tag{30}$$

Therefore, considering Eq. (18) and combining the inertial derivatives of $\mathbf{h}_B$, $\mathbf{h}_G$ and $\mathbf{h}_W$, the equation of motion of the 3D pendulum with a VSCMG is given by

$$\begin{aligned}[I]\dot{\boldsymbol{\omega}} =& -\boldsymbol{\omega} \times [I]\boldsymbol{\omega} - \hat{\mathbf{g}}_s(J_s\dot{\gamma}\omega_t + I_{ws}\dot{\Omega} - (J_t - J_g)\omega_t\dot{\gamma}) \\ &- \hat{\mathbf{g}}_t\left((J_s\omega_s + I_{ws}\Omega)\dot{\gamma} - (J_t + J_g)\omega_s\dot{\gamma} + I_{ws}\Omega\omega_g\right) \\ &- \hat{\mathbf{g}}_g(J_g\ddot{\gamma} - I_{ws}\Omega\omega_t) + \boldsymbol{\ell}.\end{aligned} \tag{31}$$

In this format, the inertia matrices were combined as presented in Eq. (10). The expression presented in Eq. (31) can be more simplified if we consider $J_s \approx I_{ws}$ once the gimbal frame inertia I_{Gs} is usually very small and can be neglected when compared to I_{ws}. Therefore, the equation of motion of the 3D pendulum with a single VSCMG is given by

$$\begin{aligned}[I]\dot{\boldsymbol{\omega}} =& -\boldsymbol{\omega} \times [I]\boldsymbol{\omega} - \hat{\mathbf{g}}_s\left(J_s(\dot{\Omega} + \dot{\gamma}\omega_t) - (J_t - J_g)\omega_t\dot{\gamma}\right) \\ &- \hat{\mathbf{g}}_t\left(J_s(\omega_s + \Omega)\dot{\gamma} - (J_t + J_g)\omega_s\dot{\gamma} + J_s\Omega\omega_g\right) \\ &- \hat{\mathbf{g}}_g(J_g\ddot{\gamma} - J_s\Omega\omega_t) + \boldsymbol{\ell}.\end{aligned} \tag{32}$$

The complete model of the 3D pendulum with VSCMG has to be solved. This model encompasses the kinematic differential equation given in Eq. (6), the equation of motion presented in Eq. (32), and the motor torque Eqs. (26) and (29).

2.4 Dynamic analysis

References [2] and [16] have shown that the 3D pendulum presents two equilibrium manifolds. The hanging equilibrium occurs when the center of mass of the pendulum is below the pivot. The inverted equilibrium occurs when the center of mass is directly above the pivot. Shen et al. [2] have proven that the hanging equilibrium is stable in the sense of Lyapunov and that the inverted is unstable.

2.5 Assumptions to model the spherical pendulum

As aforementioned, the objective is to control a spherical pendulum with a VSCMG. The alternative found to model this pendulum configuration was to derive a general model for a 3D pendulum and, based on the assumptions made in [2, 16], to obtain a spherical pendulum.

The assumptions considered to yield the spherical pendulum are: (1) the rigid pendulum is axis symmetric; (2) the pivot is located in the axis of symmetry; and (3) the body has only two possible rotations. Therefore, the angular velocity ω_3 of the body around $\hat{b}_3$ is assumed to be zero. This leads to $\dot{\omega}_3 = 0$.

2.6 Error dynamics

After deriving the mathematical model of the 3D pendulum with a VSCMG and showing how to obtain a spherical pendulum from that model, now we need to obtain the error dynamics that is used in the controller design.

Let us first define the error attitude matrix as

$$[\tilde{D}] = [BN][RN]^T, \tag{33}$$

where $[RN]^T$ is the attitude matrix of the reference frame R w.r.t. the inertial one. The error MRP $\tilde{\boldsymbol{\sigma}}$ can be extracted from the attitude error matrix as

$$\tilde{\boldsymbol{\sigma}} = \frac{1}{\zeta(\zeta+2)}\begin{bmatrix} \tilde{D}_{23} - \tilde{D}_{32} \\ \tilde{D}_{31} - \tilde{D}_{13} \\ \tilde{D}_{12} - \tilde{D}_{21} \end{bmatrix}, \tag{34}$$

where $\zeta = \sqrt{\text{trace}\,(\tilde{\mathbf{D}}) + 1}$ and $\tilde{D}_{ij}$ denote the elements of the ith row and jth column of $[\tilde{D}]$. The attitude error kinematic differential equation of the MRPs is given in the same form as presented in Eq. (6).

The angular velocity error is defined as

$$\tilde{\boldsymbol{\omega}} = \boldsymbol{\omega} - [\tilde{D}]\boldsymbol{\omega}_r, \tag{35}$$

where $\boldsymbol{\omega}_r \triangleq^R \boldsymbol{\omega}_{r/n}$ is the angular velocity command.

3 Controller design

This section presents the derivation of a feedback control law suitable for using the favorable aspects of the VSCMG to control the spherical pendulum. To design the control strategy, the following Lyapunov candidate function is selected

$$V(\tilde{\boldsymbol{\omega}}, \tilde{\boldsymbol{\sigma}}) = \frac{1}{2}\tilde{\boldsymbol{\omega}}^T[I]\tilde{\boldsymbol{\omega}} + 2Kln(1 + \tilde{\boldsymbol{\sigma}}^T\tilde{\boldsymbol{\sigma}}), \tag{36}$$

which is positive definite and radially unbounded once K is a positive attitude feedback gain and the inertia matrix $[I]$ is a positive definite matrix.

The time derivative of the Lyapunov candidate function presented in Eq. (36) is given by

$$\dot{V}(\tilde{\boldsymbol{\omega}}, \tilde{\boldsymbol{\sigma}}) = \tilde{\boldsymbol{\omega}}^T\left([I]\frac{^B\mathrm{d}}{\mathrm{dt}}(\tilde{\boldsymbol{\omega}}) + \frac{1}{2}\frac{^B\mathrm{d}}{\mathrm{dt}}([I])\tilde{\boldsymbol{\omega}} + K\tilde{\boldsymbol{\sigma}}\right). \tag{37}$$

It is important to note that for this case the inertia matrix $[I]$ is time-varying. This happens because of the CMG gimballing. Let us recall that the Lyapunov function is a scalar quantity, thus the derivative involves only the scalar components. The derivatives of $[I]$ and $\tilde{\boldsymbol{\omega}}$ are evaluated as seen by the B frame. The derivative of the inertia matrix in the B frame is given by

$$\frac{^B\mathrm{d}}{\mathrm{dt}}([I]) = \dot{\gamma}(J_s - J_t)(\hat{\mathbf{g}}_s\hat{\mathbf{g}}_t^T + \hat{\mathbf{g}}_t\hat{\mathbf{g}}_s^T). \tag{38}$$

Based on the Lyapunov theory, $\dot{V}$ is required to be negative semi-definite in order to guarantee stability. Thus, the rate of the Lyapunov candidate function is forced to be negative semi-definite as

$$\dot{V} = -\tilde{\boldsymbol{\omega}}^T[P]\tilde{\boldsymbol{\omega}}, \tag{39}$$

where $[P]$ is a positive-definite gain matrix. Combining equations (37) with (39), we obtain following stability condition

$$[I]\frac{^B\mathrm{d}}{\mathrm{dt}}(\tilde{\boldsymbol{\omega}}) = -K\tilde{\boldsymbol{\sigma}} - [P]\tilde{\boldsymbol{\omega}} - \frac{1}{2}\frac{^B\mathrm{d}}{\mathrm{dt}}([I])\tilde{\boldsymbol{\omega}}. \tag{40}$$

Substituting the equation of motion of the 3D pendulum with a VSCMG, presented in Eq. (32), and the derivative of the inertia matrix, given by Eq. (38), into (40), and after some algebraic manipulations, the stability condition can be written as

$$\begin{aligned} &J_s\dot{\Omega}\hat{\mathbf{g}}_s + J_g\ddot{\gamma}\hat{\mathbf{g}}_g + \dot{\gamma}(J_s\Omega\hat{\mathbf{g}}_t + \frac{1}{2}(J_s - J_t)(\omega_t\hat{\mathbf{g}}_s + \omega_s\hat{\mathbf{g}}_t) \\ &\quad + J_g(\omega_t\hat{\mathbf{g}}_s - \omega_s\hat{\mathbf{g}}_t) + \frac{1}{2}(J_s - J_t)(\hat{\mathbf{g}}_s\hat{\mathbf{g}}_t^T\boldsymbol{\omega}_r + \hat{\mathbf{g}}_t\hat{\mathbf{g}}_s^T\boldsymbol{\omega}_r)) = \\ &K\tilde{\boldsymbol{\sigma}} + [P]\tilde{\boldsymbol{\omega}} + \boldsymbol{\ell} - [\boldsymbol{\omega}\times][I]\boldsymbol{\omega} - [I](\dot{\boldsymbol{\omega}}_r - [\boldsymbol{\omega}\times]\boldsymbol{\omega}) \\ &\quad - J_s\left(\Omega\omega_g\hat{\mathbf{g}}_t - \Omega\omega_t\hat{\mathbf{g}}_g\right). \end{aligned} \tag{41}$$

For simplicity of notation, the following quantities are defined

$$[D_0] \triangleq [J_s\hat{\mathbf{g}}_s], \tag{42}$$

$$[D_1] \triangleq \left[J_s\left((\Omega + \frac{1}{2}\omega_s)\hat{\mathbf{g}}_t + \frac{1}{2}\omega_t\hat{\mathbf{g}}_s\right)\right], \tag{43}$$

$$[D_2] \triangleq \left[\frac{1}{2}J_t\left(\omega_t\hat{\mathbf{g}}_s + \omega_s\hat{\mathbf{g}}_t\right)\right], \tag{44}$$

$$[D_3] \triangleq [J_g(\omega_t\hat{\mathbf{g}}_s - \omega_s\hat{\mathbf{g}}_t)], \tag{45}$$

$$[D_4] \triangleq \left[\frac{1}{2}(J_s - J_t)(\hat{\mathbf{g}}_s\hat{\mathbf{g}}_t^T + \hat{\mathbf{g}}_t\hat{\mathbf{g}}_s^T)\boldsymbol{\omega}_r\right], \tag{46}$$

$$[B] \triangleq [J_g\hat{\mathbf{g}}_g]. \tag{47}$$

Thus, the stability condition in a compact form similarly to the one adopted in reference [31] is

$$[D_0]\dot{\Omega} + [B]\ddot{\gamma} + [D]\dot{\gamma} = \boldsymbol{\ell}_r, \tag{48}$$

where $[D] = [D_1] - [D_2] + [D_3] + [D_4]$ and the required torque vector $\boldsymbol{\ell}_r$ is given by:

$$\begin{aligned}\boldsymbol{\ell}_r =& K\tilde{\boldsymbol{\sigma}} + [P]\tilde{\boldsymbol{\omega}} + \boldsymbol{\ell} - [\boldsymbol{\omega}\times][I]\boldsymbol{\omega} - [I](\dot{\boldsymbol{\omega}}_r - [\boldsymbol{\omega}\times]\boldsymbol{\omega}) + \\ &- J_s\left(\Omega\omega_g\hat{\mathbf{g}}_t - \Omega\omega_t\hat{\mathbf{g}}_g\right).\end{aligned} \tag{49}$$

The proof of stability of this control law is analogous to the one presented in reference [31]. Note that the Lyapunov function rate was set to be only negative semi-definite, thereby, from the stability condition, at this stage, we can infer that the proposed control scheme only assures global stability in the sense of Lyapunov. However, it is clear from Eq. (39) that the angular velocity error converge to zero as time evolves. To assure that the proposed control law is stabilizing the system in global-asymptotic sense, the higher-order derivatives of the Lyapunov function are investigated as done in previous works [7, 11, 31, 32], using the theorem provided in reference [33], which states that if the first nonzero higher-order derivative of V, evaluated on the set of states such that V is zero, is of an odd order and negative definite, then the origin is asymptotically stable.

If $\tilde{\boldsymbol{\omega}}$ is zero, then $\dot{V}$ is also zero. Evaluating the second-order derivative $\ddot{V}$ yields

$$\ddot{V} = -2\tilde{\boldsymbol{\omega}}^T[P]\dot{\tilde{\boldsymbol{\omega}}}. \tag{50}$$

Analyzing Eq. (50) when $\tilde{\boldsymbol{\omega}} = 0$, it yields $\ddot{V} = 0$, nothing can be concluded regarding the stability. Thus, the third derivative is evaluated

$$\dddot{V} = -2\tilde{\boldsymbol{\omega}}^T[P]\ddot{\tilde{\boldsymbol{\omega}}} - 2\dot{\tilde{\boldsymbol{\omega}}}^T[P]\dot{\tilde{\boldsymbol{\omega}}}. \tag{51}$$

For the sake of simplicity, $\dot{\tilde{\boldsymbol{\omega}}}$ is used instead of $\frac{^B\mathrm{d}}{\mathrm{dt}}(\tilde{\boldsymbol{\omega}})$. From Eq. (40), we have

$$\dot{\tilde{\boldsymbol{\omega}}} = -[I]^{-1}K\tilde{\boldsymbol{\sigma}}. \tag{52}$$

Now, substituting Eq. (52) into Eq. (51) and assigning $\tilde{\boldsymbol{\omega}} = 0$, we obtain

$$\dddot{V}(\tilde{\boldsymbol{\sigma}}, \tilde{\boldsymbol{\omega}} = 0) = -2K^2\tilde{\boldsymbol{\sigma}}^T[I]^{-1}[P][I]^{-1}\tilde{\boldsymbol{\sigma}}, \tag{53}$$

which is negative definite once $[I]$ and $[P]$ are positive definite matrices. Thus, the global asymptotic stability is guaranteed.

3.1 Control law

The gimbal and reaction wheel motor torques do not appear directly on the stability condition presented in Eq. (48). Only the rate and acceleration of the gimbal, and reaction wheel acceleration appear. To include the motor torques in the stability condition would yield equivalent control laws. However, some undesirable terms would show up that provides excessive gimbal rates. Besides, CMGs usually require the gimbal rate as input [31]. The objective is to use favorably the torque produced by the reaction wheel and the torque amplification feature that the gyroscopic torque produces when the reaction wheel is gimballed.

To do so, the term $[B]\ddot{\gamma}$ is dropped to avoid torque being generated mainly through this term since that in the $[B]$ term, the inertia J_g is generally smaller than the ones in the spin direction J_s. This leads to higher gimbal angular accelerations $\ddot{\gamma}$, which would make the CMG works as a reaction wheel and the torque amplification effect that the CMG provides would not be deeply exploited. Thereby, the stability condition can be rewritten as

$$[D_0]\dot{\Omega} + [D]\dot{\gamma} = \boldsymbol{\ell}_r. \tag{54}$$

To simplify the notation, the state vector $\boldsymbol{\eta} = \{\Omega\ \gamma\}^T$, and the matrix $[Q] = [D_0\ D_1]$ are introduced. Thus, Eq. (54) can be written as

$$[Q]\dot{\boldsymbol{\eta}} = \boldsymbol{\ell}_r. \tag{55}$$

Equation (55) provides the kinematic directive for the VSCMG, and some of the traditional CMG singularities can be avoided when the reaction wheel angular velocity is changed. To evaluate the desired rates for the gimbal and for the reaction wheel, the weighted pseudo-inverse matrix of $[Q]$ is recommended to be used as done in references [31, 32]:

$$\dot{\boldsymbol{\eta}} = [W][Q]^T\left([Q][W][Q]^T\right)^{-1}\boldsymbol{\ell}_r, \tag{56}$$

with $[W] = \mathrm{diag}\,(W_s, W_g)$, where W_s is the weight of the reaction wheel mode and W_g is the weight of the gimbal mode. None specific criterion is used here, the designer should choose these weights, thus, allowing to specify how active each control action is. For instance, the control mode of the reaction wheel can be turned off and the reaction wheel speed held constant. Therefore, the VSCMG should act as a traditional CMG.

The control law as shown here does not use any mechanism to avoid CMG singularities or to verify if the CMG configuration is close to a singularity. The only feature explored is that if the CMG cannot exert any torque to the pendulum, the reaction wheel can produce torque since the spin up or down of it is allowed in the VSCMG mechanism.

3.2 Torque level control

As stated before, the motor torques of the gimbal and of the reaction wheel do not appear in the designed control law. Therefore, the control law's subservo control must be investigated to yield a torque-level control command once the control law provides only kinematic directive. Thereby,

the servo control for the CMG and for the reaction is developed in this subsection.

Consider the motor torque equation of the gimbal presented in Eq. (29). A simplification is made to the motor torque equation of the gimbal, since $\dot{\boldsymbol{\omega}}$ is usually much smaller than the gimbal rates, this term is dropped. This simplification reduces the complexity of the servo control once $\dot{\boldsymbol{\omega}}$ and $\ddot{\gamma}$ would have to be solved together to provide the gimbal motor torque. The gimbal motor torque equation is simplified to

$$u_g = J_g\ddot{\gamma} - (J_s - J_t)\omega_s\omega_t - I_{ws}\Omega\omega_t. \tag{57}$$

To evaluate u_g, the gimbal angular acceleration is needed. Equation (55) provides the desired gimbal rate $\dot{\gamma}_d$ that when numerically differentiated yields $\ddot{\gamma}_d$. Thus, stable servo dynamics are achieved by developing a feedback control to generate an expression for $\ddot{\gamma}$. So, the servo control for the gimbal has to determine $\ddot{\gamma}$ while $\dot{\gamma}$ approaches $\dot{\gamma}_d$. The following Lyapunov function is chosed

$$V(\Delta\dot{\gamma}) = \frac{1}{2}\Delta\dot{\gamma}, \tag{58}$$

being positive definite, and the tracking error is denoted by $\Delta\dot{\gamma} \triangleq \dot{\gamma} - \dot{\gamma}_d$. The derivative of the Lyapunov function is evaluated and forced to be negative define, yielding

$$\dot{V} = \Delta\dot{\gamma}\delta\ddot{\gamma} = -K_\gamma\Delta\dot{\gamma}^2, \tag{59}$$

where K_γ is a positive gain. The expression for the gimbal angular acceleration is given by

$$\ddot{\gamma} = \ddot{\gamma}_d - K_\gamma\Delta\dot{\gamma}. \tag{60}$$

This expression is then substituted into Eq. (57), leading to the gimbal rate servo control torque

$$u_g = J_g(\ddot{\gamma}_d - K_\gamma\Delta\dot{\gamma}) - (J_s - J_t)\omega_s\omega_t - I_{ws}\Omega\omega_t. \tag{61}$$

The servo control for the reaction wheel is developed analogously. Consider the reaction wheel motor equation shown in Eq.(26). The same arguments are used to simplify the motor torque equation of the reaction wheel to

$$u_s = I_{ws}(\dot{\Omega} + \dot{\gamma}\omega_t). \tag{62}$$

Carrying out the same procedure, the following reaction wheel torque control is obtained:

$$u_s = I_{ws}(\dot{\Omega}_d - K_\Omega\Delta\Omega + \dot{\gamma}\omega_t), \tag{63}$$

where K_Ω is a positive gain and the velocity tracking error is $\Delta\Omega \triangleq \Omega - \Omega_d$.

An important remark is that the servo control needs to be faster than the attitude control loop, *i.e.*, it needs to be updated at a higher frequency with appropriate gains and parameters.

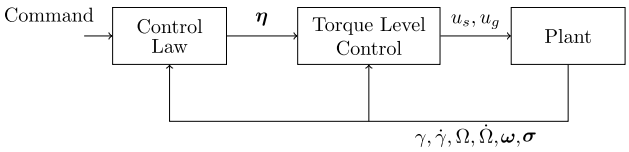

Fig. 2 Block diagram of the control loop for the spherical pendulum with a VSCMG

Figure 2 illustrates the block diagram of the complete control set-up.

With the reference and actual rates, the attitude and angular velocity errors are evaluated. These two quantities and the actual states of the spherical pendulum with a VSCMG are used as inputs for the control law. At this stage, the designer has already decided which are the weights for the gimbal and for the reaction wheel. Thus, the control law calculates the desired gimbal rate $\dot{\gamma}_d$ and $\dot{\Omega}_d$ that constitutes $\dot{\boldsymbol{\eta}}$. Then, the torque level control computes the motor torques for the gimbal and for the reaction that are necessary for the complete model integration. Afterward, the states are fed back and the process is restarted.

4 Numerical results

This section brings forward the numerical results to evaluate the proposed spherical pendulum with a VSCMG. Here, two scenarios are investigated. First, we drive the spherical pendulum to a sequence of attitude commands. In the second scenario, we choose to track a desired reference.

Based on references [18, 31], the physical parameters used in the numerical simulations are $m = 30.5$ kg, $[I_s] =$ diag $(5.3, 5.3, 14.5)$ kgm^2, ${}^G[J] =$ diag $(0.13, 0.04, 0.03)$ kgm^2, and $\mathbf{r}_{CM} = (0, 0, 0.22)$ m. The gains used for the controller are $K = 400, [P] =$ diag $(50, 50, 50)$, $K_\gamma = 2$, and $K_\Omega = 1$. Furthermore, the weights are chosen as $W_s = 2$ and $W_g = 1$. The script was coded in MATLAB using the Euler integration method with a time step of 0.001 s. For all the numerical simulations performed, we have used the initial conditions as Euler angles in the 1-2-3 sequence $(-25°, -25°, 0)$ for the attitude which is converted to an attitude matrix from which the initial MRP is extracted. For the VSCMG, we consider $\gamma(0) = 30°$ and $\Omega(0) = 72$ rad/s. To verify the robustness of the controller, we have considered a random disturbance torque with uniform distribution between -3 and 3 Nm for both cases investigated.

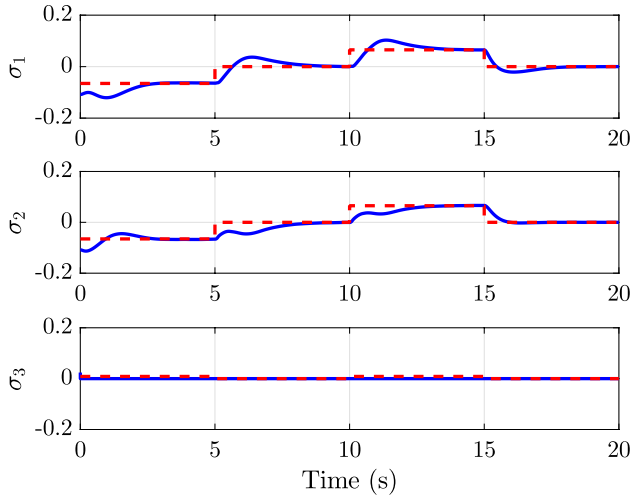

Fig. 3 Controlled attitude for a sequence of attitude commands, - - - indicates the reference

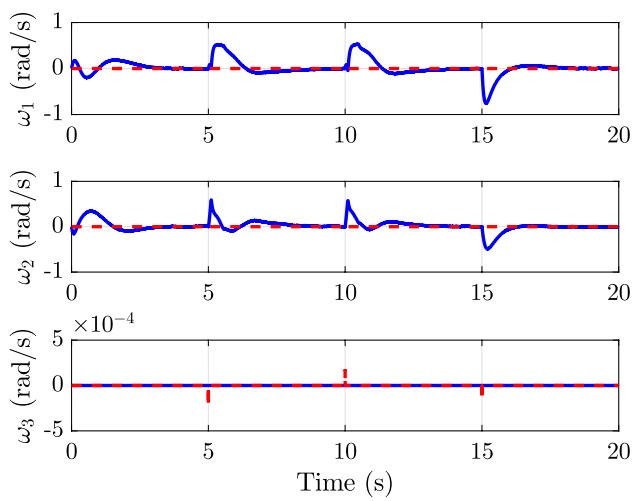

Fig. 4 Controlled body angular velocity for a sequence of attitude commands, - - - indicates the reference

4.1 Controlling the spherical pendulum with a VSCMG in a sequence of attitude commands

This subsection presents the numerical results for driving the pendulum to a sequence of attitude commands including the upright position. To do so, we set the commands in Euler angles in the 1-2-3 sequence, where the first attitude is $(-15°, -15°, 0)$, the second one is $(0, 0, 0)$, the third one is $(15°, 15°, 0)$, and the final one is $(0, 0, 0)$. Note that based on the reference system we have adopted, the attitude $(0, 0, 0)$ represents the upright position. The changes in the attitude commands occur every 5 sec.

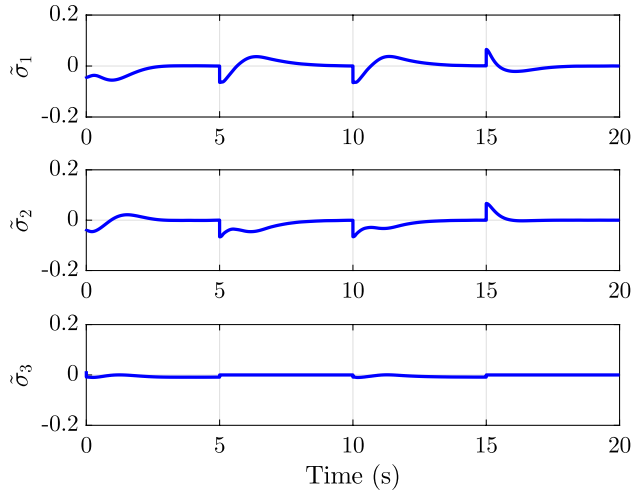

Fig. 5 Attitude error for a sequence of attitude commands

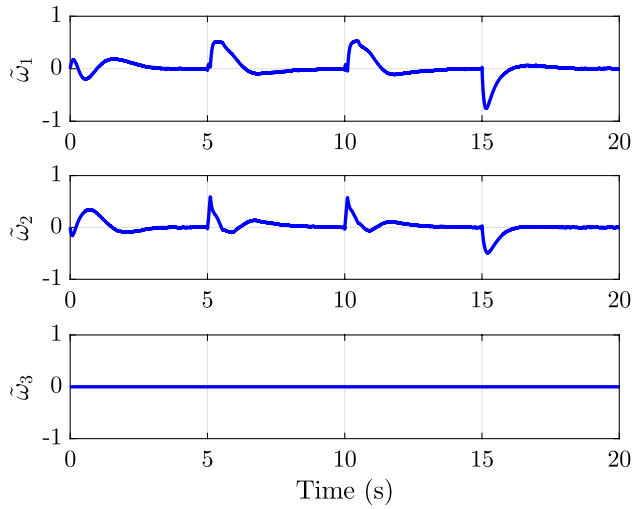

Fig. 6 Angular velocity error for a sequence of attitude commands

Figure 3 presents the controlled attitude given in terms of the MRPs, where we can note that before 5 sec the spherical pendulum is controlled in the first attitude command. Then, at 5 sec the reference is changed, and the pendulum is taken to the new desired attitude, which is repeated until the final attitude command, where the pendulum returns to the upright position.

Figure 4 shows the body angular velocity for this case. The same behavior is observed here, the angular velocities go to zero before 5 sec, in the sequel, the attitude command is changed every 5 sec and the controller is able to bring the body angular velocity back to zero every time. One important thing to note here is that the third component is kept at zero for all simulation time. This is due to

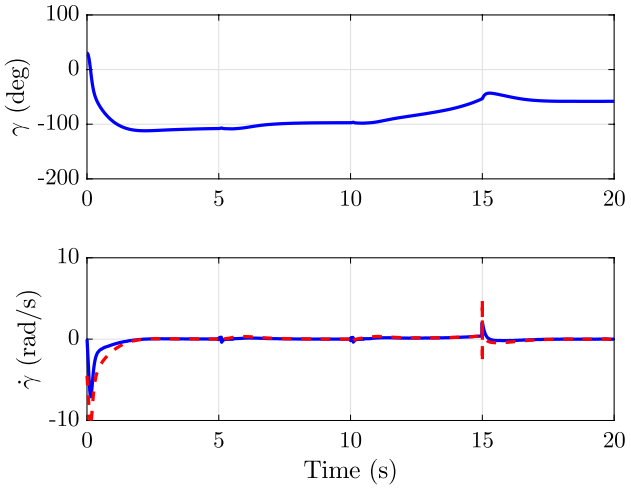

Fig. 7 Gimbal rates for controlling the pendulum in a sequence of attitude commands, - - - indicates the commanded gimbal rate

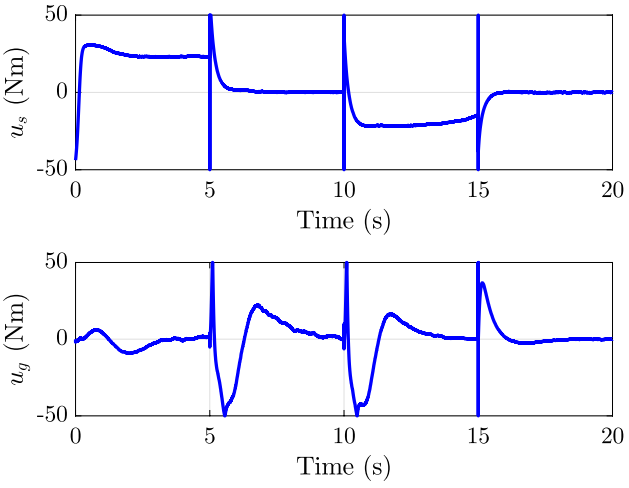

Fig. 9 Reaction wheel and gimbal motor torques for controlling the pendulum in a sequence of attitude commands

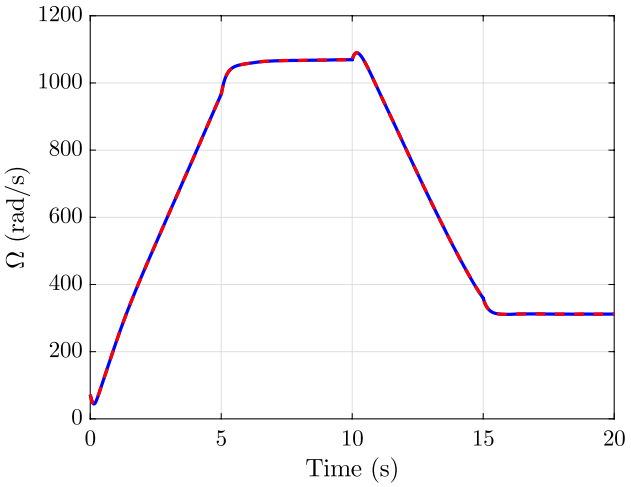

Fig. 8 Reaction wheel angular velocity for controlling the pendulum in a sequence of attitude commands, - - - indicates the commanded reaction wheel angular velocity

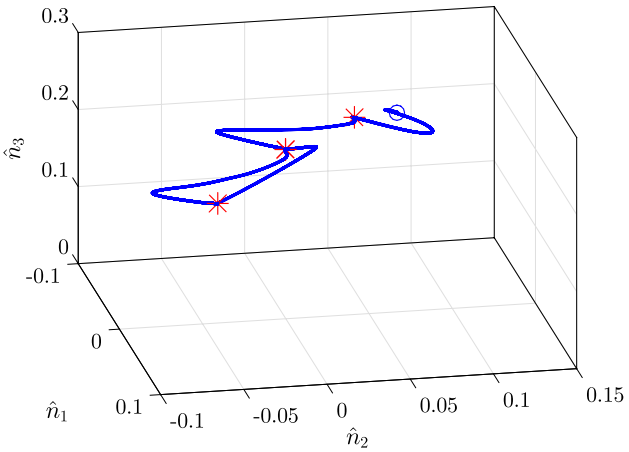

Fig. 10 Position of the center of mass for controlling the pendulum in a sequence of attitude commands. ∘ represents the initial condition and ∗ indicates attitude commands

one of the assumptions carried out to yield the spherical pendulum where it is not allowed to rotate around $\hat{b}_3$.

Figures 5 and 6 depict the attitude and angular velocity errors, respectively. We can observe that the tracking errors using the proposed controller go to values very close to zero when the commanded reference is reached and a small oscillation due to disturbance applied can be observed.

Figure 7 illustrates the gimbal rates, where we can see that the gimbal presents smooth motions when the desired attitude commands are changed, exemplifying the torque amplification feature of the CMGs. Furthermore, note that when the pendulum reaches the equilibrium in the upright position, the gimbal angle (γ) goes to a fixed position and stays there.

Figure 8 exhibits the reaction wheel angular velocity that also converge to a constant value after the pendulum reaches the upright position, which can be noted after 16 sec. We can also observe that the actual rates for the VSCMG are close to the desired rates generated by the control law for the gimbal as well as for the reaction wheel.

Figure 9 presents the motor torques for the reaction wheel and for the gimbal. Although these values might appear to have a large magnitude, they are consistent with the physical parameters used for the numerical simulations of the spherical pendulum with a VSCMG which are high values. The influence of the random disturbance torque can also be

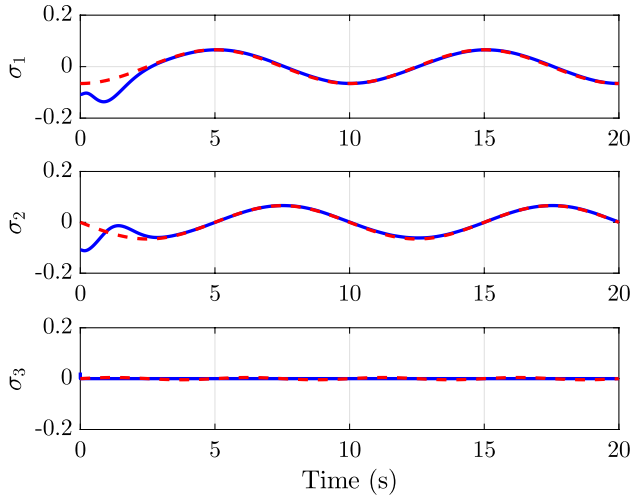

Fig. 11 Controlled attitude for tracking a desired reference, - - - indicates the reference

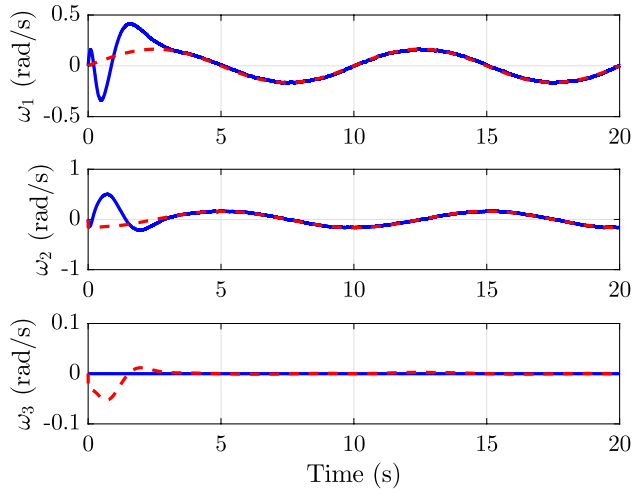

Fig. 12 Controlled body angular velocity for tracking a desired reference, - - - indicates the reference

observed in the reaction wheel and gimbal motor torques where some oscillations can be noted. These small oscillations are produced in order to the actuators to deal with the external disturbances applied to the system. The spikes depicted in both figures are due to the sudden change of the attitude command.

Moreover, for a better visualization of the result, the motion of the center of mass vector is presented in Fig. 10.

The MRPs are not very intuitive to evaluate the motion of a dynamic system although presenting very elegant properties. Therefore, analyzing Fig. 10 one can see that the initial condition chosen is not very far from the upright position and it is represented by a blue circle. This was done in order to avoid non-physical motions, i.e., motions that might be impossible to reproduce in practical experiments, taking into account the possible limitations of a future experimental setup. The attitude commands can also be observed in Fig. 10, depicted in red asterisks. From right to left, the pendulum leaves the initial condition and goes to the first attitude command, and then, to the second one in the center. After that, it goes to the one at the far left and it is driven back to the central one that represents the upright position. Thus, we can see that the spherical pendulum is taken to a sequence of attitude commands including the upright position using the favorable aspects of the VSCMG.

4.2 Tracking a desired reference

This subsection shows the results obtained for tracking a desired reference for the spherical pendulum with a VSCMG. In this case, we have set the desired reference as Euler angles in the 1-2-3 sequence given by $(15° \sin(2\pi f_c t - \pi/2),\ 15° \sin(2\pi f_c t - \pi),\ 0)$ with $f_c = 0.1$ Hz which is converted for MRPs. The controlled attitude given in terms of the MRPs is depicted in Fig. 11, where we can observe that the proposed control law makes the system follow the desired reference.

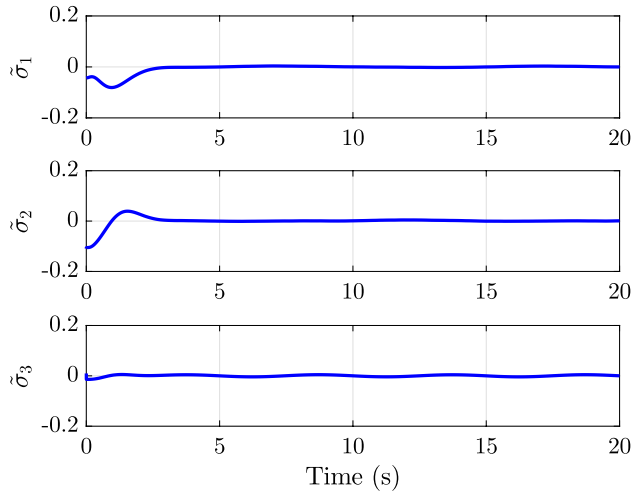

Fig. 13 Attitude error for tracking a desired reference

Figure 12 exhibits the body angular velocities for this case, where we can also note that the controller can track the desired angular velocity well.

Figure 13 illustrates the attitude error for tracking a desired reference using the proposed controller. Note that the attitude errors represented in terms of the MRPs converge to values close to zero after a few seconds.

Figure 14 presents the angular velocity errors that also converge to values close to zero after a few seconds. Small oscillations due to the random uniform disturbance torque applied can be noted in the angular velocity error.

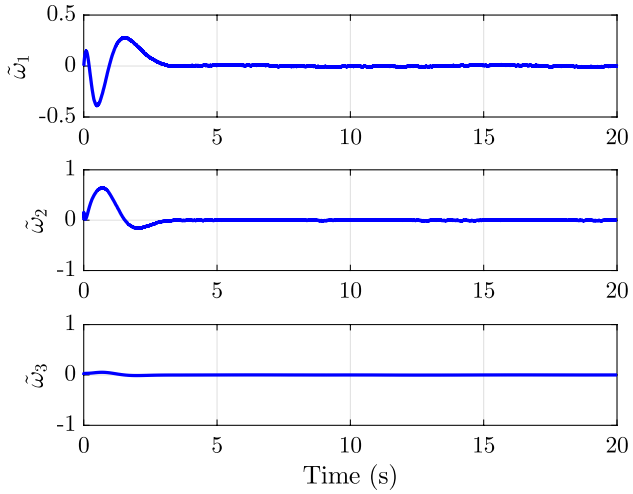

Fig. 14 Angular velocity error for tracking a desired reference

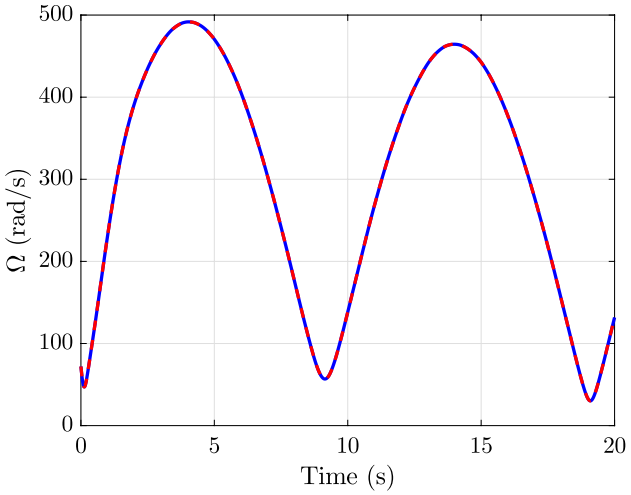

Fig. 16 Reaction wheel angular velocity for tracking a desired reference, - - - indicates the commanded reaction wheel angular velocity

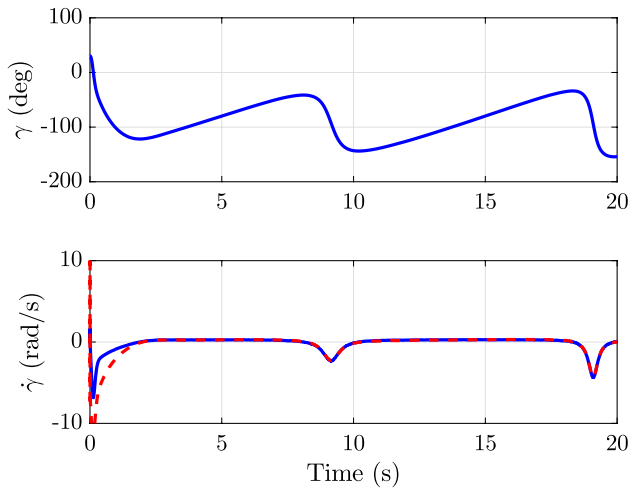

Fig. 15 Gimbal rates for tracking a desired reference, - - - indicates the commanded gimbal rate

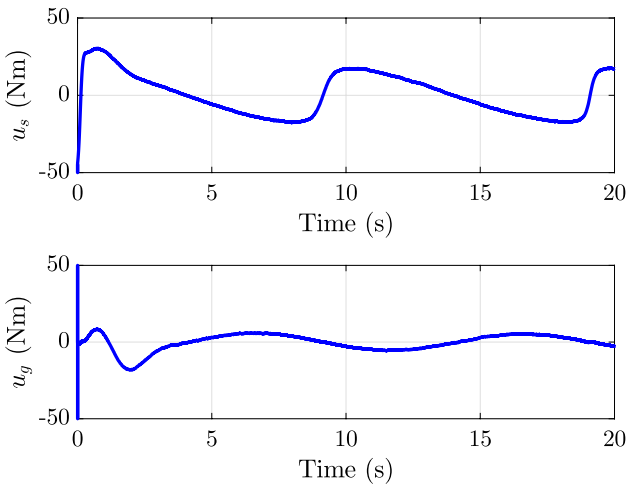

Fig. 17 Reaction wheel and gimbal motor torques for tracking a desired reference

Figure 15 shows the gimbal rates for this case. Note that the gimbal has to move during the control process in order to produce the required torque once the reference is time-varying. Furthermore, it is important to observe that for this case the gimbal motion is also smooth, which can be seen in the gimbal angle (γ).

The reaction wheel angular velocity is depicted in Fig. 16. The reaction wheel and gimbal motor torques for this cases are presented in Fig. 17. As aforementioned, one of the goals is to use the gyroscopic torque combined with the reaction wheel torque. Figures 15, 16, and 17 help us to visualize such phenomena. Besides, the reaction wheel works within reasonable rates, i.e., these rates can be reproduced in a practical experiment. Although large torques are demanded at the beginning of the simulation, it is imperative to take into account that the body, i.e., the pendulum has a large mass and a large inertia. The controller has also to deal with the torque caused by gravity. Thus, the motor torques of the gimbal and reaction wheel also yield reasonable values.

Once again for a better visualization of the results, we depict in Fig. 18 the position of the center of mass of the spherical pendulum with a VSCMG. Note that the proposed approach can track a desired reference with adequate performance.

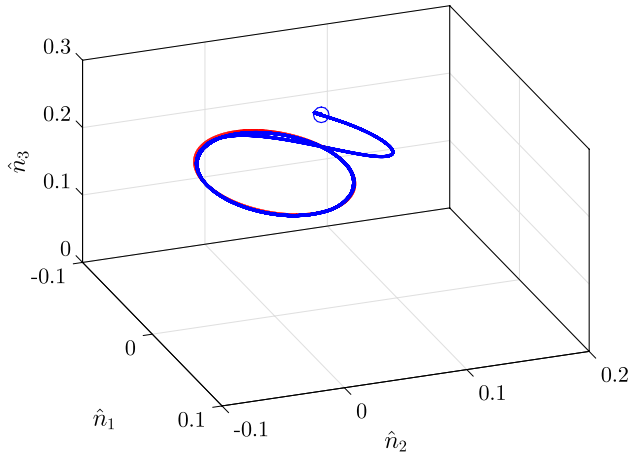

Fig. 18 Position of the center of mass for tracking a desired reference, where ∘ indicates the initial condition

5 Final Remarks

This paper has introduced the complete modeling of a spherical pendulum with a VSCMG, based on the 3D pendulum model. This was done taking into account some assumptions presented in the literature, which are to provide an axis-symmetric inertia matrix for the 3D pendulum and to allow no rotation around $\hat{\boldsymbol{b}}_3$, i.e., $\omega_3 = 0$, which leads to $\dot{\omega}_3 = 0$. A nonlinear controller suitable for such dynamic system has been derived. The control law designed assures global asymptotic stability. Furthermore, the numerical results presented reasonable rates for driving the spherical pendulum to a sequence of attitude commands including the upright position as well as to track a desired reference. Favorable aspects of using a VSCMG are well employed in the control of the spherical pendulum using the gyroscopic torque combined with the reaction wheel torque. To the best of our knowledge, the VSCMG-actuated spherical pendulum has not been deeply studied as presented in this paper. Furthermore, in the cases studied by this paper, the proposed model has provided a nonsingular model for the spherical pendulum and no CMG singularities were reached.

Acknowledgements The authors thank the São Paulo Research Foundation (FAPESP) for the financial support (Grants 2017/12985-2, 2018/13751-8, and 2020/12314-3). The second and third author are also grateful for the support of National Council of Technological and Scientific Development (CNPq) (Grants 304300/2021-7, and 306526/2019-0).

Declarations

Conflict of interest The authors declare that they have no conflict of interest.

References

1. Spong MW, Corke P, Lozano R (2001) Nonlinear control of the reaction wheel pendulum. Automatica 37(11):1845–1851
2. Shen J, Sanyal AK, Chaturvedi NA, Bernstein D, McClamroch H (2004) Dynamics and control of a 3D pendulum. In: IEEE conference on decision and control, CDC, 43, vol 1, pp 323–328, Nassau: IEEE, (IEEE Cat. No. 04CH37601)
3. Pathak K, Franch J, Agrawal SK (2005) Velocity and position control of a wheeled inverted pendulum by partial feedback linearization. IEEE Trans Rob 21(3):505–513
4. Sanyal Amit K, Ambarish G (2013) Dynamics and balance control of the reaction mass pendulum: a three-dimensional multibody pendulum with variable body inertia. J Dyn Sys Meas Control 136(2):021002
5. Muehlebach M, DÁndrea R (2017) Nonlinear analysis and control of a reaction-wheel-based 3-D inverted pendulum. IEEE Trans Control Syst Technol 25(1):235–246
6. Déda T, Fujiwara E, Carneiro E (2018) Modular approach for control design of an autonomous two-wheeled inverted pendulum. J Braz Soc Mech Sci Eng 40(11):536
7. Trentin JFS, da Silva S, Schaub H (2019) Variable speed control moment gyroscope in an inverted pendulum. J Dyn Syst Meas Contr 141(11):111012
8. Trentin JFS, Cenale TP, da Silva S, de Souza Ribeiro JM (2019) Attitude control of inverted pendulums using reaction wheels: comparison between using one and two actuators. Proc Inst Mech Eng Part I J Syst Control Eng 234(3):420–429
9. Trentin JFS, Da Silva S, De Souza Ribeiro JM, Schaub H (2020) Inverted pendulum nonlinear controllers using two reaction wheels: design and implementation. IEEE Access 8:74922–74932
10. Bayram A, Kara F (2020) Design and control of spatial inverted pendulum with two degrees of freedom. J Braz Soc Mech Sci Eng 42(10):501
11. Trentin JFS (2020) Attitude control of inverted pendulums using reaction wheels and variable speed control moment gyroscope. PhD thesis, São Paulo State University (UNESP), School of Engineering of Ilha Solteira
12. Trentin JFS, da Silva S, de S Ribeiro JM, Schaub H (2021) An experimental study to swing up and control a pendulum with two reaction wheels. Meccanica 56(4):981–990
13. Chaturvedi NA, Bacconi F, Sanyal AK, Bernstein D, McClamroch NH (2005) Stabilization of a 3D rigid pendulum. In: Proceedings of the 2005, American Control Conference, 2005., pp 3030–3035, vol. 5
14. Chaturvedi NA, McClamroch NH (2007) Asymptotic stabilization of the hanging equilibrium manifold of the 3d pendulum. Int J Robust Nonlinear Control 17(16):1435–1454
15. Chaturvedi NA, McClamroch NH (2007) Attitude stabilization of the inverted 3D pendulum on tso(3) with control saturation. In: 46th IEEE conference on decision and control, pp 1910–1915
16. Chaturvedi NA, McClamroch NH, Bernstein DS (2008) Stabilization of a 3D axially symmetric pendulum. Automatica 44(9):2258–2265
17. Zou K, Ge X (2017) Neural-network-based fuzzy logic control of a 3d rigid pendulum. Int J Control Autom Syst 15(5):2425–2435
18. Yao Q (2020) Robust adaptive finite-time attitude tracking control of a 3D pendulum with external disturbance: numerical simulations and hardware experiments. Nonlinear Dyn 102:223–239
19. Gajamohan M, Merz M, Thommen I, D'Andrea R (2012) The cubli: a cube that can jump up and balance. In: International conference on intelligent robots and systems, pp 3722–3727
20. Zhu Y, Gao Y, Xu C, Zhao J, Jin H, Lee J (2015) Adaptive control of a gyroscopically stabilized pendulum and its application

to a single-wheel pendulum robot. IEEE/ASME Trans Mechatron 20(5):2095–2106
21. Jin H, Yang D, Liu Z, Zang X, Li G, Zhu Y (2015) A gyroscope-based inverted pendulum with application to posture stabilization of bicycle vehicle. In: 2015 IEEE international conference on robotics and biomimetics (ROBIO), pp 2103–2108
22. Chih-Keng Chen, Trung-Dung Chu, Xiao-Dong Zhang (2019) Modeling and control of an active stabilizing assistant system for a bicycle. Sensors 19(2):248
23. Yun SY, Lee WS, Gwak K-W (2020) Cmg-based anthropomorphic test device for human rider behavior reproduction for two-wheeled self-balancing personal mobility. Mechatronics 69:102365
24. Kim HW, Jung S (2020) Design and control of a sphere robot using a control moment gyroscope actuator for navigation. Int J Control Autom Syst 18(12):3112–3120
25. Lemus D, van Frankenhuyzen J, Vallery H (2017) Design and evaluation of a balance assistance control moment gyroscope. J. Mech Robot 9(5)
26. Lemus D, Berry A, Jabeen S, Jayaraman C, Hohl K, van der Helm FCT, Jayaraman A, Vallery H (2020) Controller synthesis and clinical exploration of wearable gyroscopic actuators to support human balance. Sci Rep 10(1):10412
27. Trung-Dung Chu, Chih-Keng Chen (2017) Design and implementation of model predictive control for a gyroscopic inverted pendulum. Appl Sci 7(12):1272
28. Aranovskiy S, Ryadchikov I, Nikulchev E, Wang J, Sokolov D (2020) Experimental comparison of velocity observers: a scissored pair control moment gyroscope case study. IEEE Access 8:21694–21702
29. Wasiwitono U, Wahjudi A, Saputra AK, Yohanes (2021) Stabilization and disturbance attenuation control of the gyroscopic inverted pendulum. J Vib Control 27(3–4):415–425
30. Zhang X, Liu Q, Liu J, Zhu Q, Huosheng H (2020) Using gyro stabilizer for active anti-rollover control of articulated wheeled loader vehicles. Proc Inst Mech Eng Part I J Syst Control Eng 235(2):237–248
31. Schaub H, Junkins JL (2014) Analytical mechanics of space systems, 3rd edn. AIAA Education Series, Reston
32. Schaub H, Vadali SR, Junkins JL (1998) Feedback control law for variable speed control moment gyros. J Astronaut Sci 46(3):307–328
33. Mukherjee R, Chen D (1993) Asymptotic stability theorem for autonomous systems. J Guid Control Dyn 16(5):961–963